THE EFFECTS OF GEOMETRY AND MATERIAL PROPERTIES ON THE FRACTURE OF SINGLE LAP-SHEAR JOINTS

M. S. Kafkalidis[1] and M. D. Thouless[1,2]

[1]*Department of Mechanical Engineering*
[2]*Department of Materials Science & Engineering*
University of Michigan
Ann Arbor, MI 48109, U.S.A.

Abstract

A review of the mechanics of lap-shear joints is followed by a detailed analysis of the problem using a cohesive-zone approach. The cohesive-zone model allows not only the influence of geometry to be considered, but also allows the cohesive properties of the interface and plastic deformation of the adherends to be included in the analysis. The first part of the paper examines the strength of elastic joints, with an emphasis on the effects of geometry, the cohesive strength of the adhesive, and mode-mixedness. The cohesive-zone models show a transition to the predictions of linear-elastic fracture mechanics under conditions where these are expected to apply. The second part of the paper examines the effect of plasticity in the adherends, and looks at the transition between the elastic and plastic regimes. The final part of the paper makes comparisons between the predictions of the numerical calculations and experimental observations for a model system consisting of a commercial adhesive used to bond an aluminum alloy. Using cohesive-zone parameters previously determined for this particular combination of materials, the numerical predictions show excellent agreement with the experimental observations.

April 2002

1. Introduction

Joints that are of the form of the single lap-shear geometry shown in Fig. 1 are of great practical importance. The behavior of such joints depends not only on the properties of the adherends and the bond between them, but also on geometrical parameters such as the length of the bonded portion of the overlap l, the total length of the specimen L, the crack length, a, and the thickness of the adherends, h. Of particular note among the models of the lap-shear geometry are the beam-bending analyses that have been developed to calculate the deformations and stresses when the adherends deform in an elastic fashion. These analyses have a particular emphasis on calculating the distribution of the bending moment along the joint [Goland and Reissner, 1944; Hart-Smith, 1973; Allman, 1977; Chen and Cheng, 1983; Tsai *et al.*, 1998]. Numerical analyses have provided further refinements to understanding the effects of the material and geometrical parameters [Adams and Peppiatt, 1974; Bigwood and Crocombe, 1989; Tsai and Morton, 1994, 1995]. A major conclusion of this body of literature is that, despite its apparent simplicity, the behavior of a lap-shear specimen is very sensitive to details of the geometry of how the specimen is loaded.

Historically, two types of analyses for the strength of lap-shear joints have been developed. One is a stress-based approach that uses the beam-bending analyses discussed in the previous paragraph to deduce stresses or strains in the adhesive layer. Failure is assumed to occur when these stresses or strains reach a critical value [Harris and Adams, 1984; Bigwood and Crocombe, 1990; Crocombe and Bigwood, 1992]. However, the use of linear-elastic fracture-mechanics (L.E.F.M.) and its energy-based approach has now gained general recognition as the most appropriate way of predicting

failure if the adherends remain elastic [Anderson *et al*., 1988; Chai, 1988; Fernlund *et al*., 1994; Papini *et al*., 1994; Tong, 1996]. Furthermore, the results of the beam-bending analyses can be used to make a connection with the work of Suo and Hutchinson [1990] for the delamination of beam-like geometries, by recognizing that an interface crack in a lap-shear specimen is acted on by a combination of axial load (per unit width), P, and bending moment (per unit width), M, as illustrated in Fig. 2 [Papini *et al.,* 1994; Lai *et al*., 1996]. If both adherends have an equal thickness, h, the bending moment, M, is proportional to Ph, but the constant of proportionality, k, is both geometry- and load-dependent [Tsai and Morton, 1995]:[1]

$$\frac{M}{Ph} = k\left(\frac{P}{Eh}, \frac{l}{h}, \frac{L}{l}\right), \tag{1}$$

where E is the elastic modulus of the adherends. For linear-elastic joints, with a crack length, a, significantly greater than h, the energy-release rate can be written as [Suo and Hutchinson, 1990]:

$$\mathcal{G} = \frac{P^2}{2Eh} + \frac{6M^2}{Eh^3} - \left[\frac{P^2}{4Eh} - \frac{12\left(M - 0.5Ph\right)^2}{16Eh^3}\right]. \tag{2}$$

So that, from Eqn. 1,

$$\mathcal{G} = \frac{P^2}{16Eh}\left[84k^2 + 12k + 1\right]. \tag{3}$$

Since k is a function of P/Eh, l/h and L/l, the complex interaction between $\mathcal{G}$, the load, and the geometry can be seen immediately. The relationship between M and P given in Eqn. 1 can also be used with the general results of Suo and Hutchinson [1990] to deduce an expression for the phase angle, ψ, of the symmetrical single lap-shear geometry:

[1] This result is for plane stress. In general, Poisson's ratio is an additional parameter that should be

$$\tan\psi = \left(\frac{\mathcal{G}_{II}}{\mathcal{G}_{I}}\right)^{1/2} = \left\{-\frac{1}{2\sqrt{3}}\left[\frac{1}{2k}+3\right]\right\} \tag{4}$$

where $\mathcal{G}_{\mathrm{I}}$ is the mode-I component of the energy-release rate and $\mathcal{G}_{\mathrm{II}}$ is the mode-II component.

There are two limiting cases for which analytical values of k can be computed. From Fig. 3a, it can be seen that k must equal 0.5 when the loads and geometry are such that negligible deformation of the sample occurs. The energy-release rate is then

$$\mathcal{G} = \frac{7P^2}{4Eh} \tag{5}$$

and the phase angle is -49.1°. However, if the geometry is long enough to be completely flexible, and the applied loads are relatively high, the free arm will deform so that its neutral axis lies along the line of action of the applied load and is, therefore, not subject to a bending moment (Fig. 3b). In this second case, there is a limiting steady-state condition in which extension of the crack does not change the geometry, and the energy-release rate can be deduced by comparing the stress state in the bonded portion of the specimen (well way from the free arm) to the stress state in the free arm (well away from the grips and bonded portion of the sample). Both portions are subjected to a uniform load of P, and the energy-release rate can then be written as

$$\mathcal{G} = \frac{P^2}{4Eh} \tag{6}$$

Hence, from Eqn. 2, it can be shown that $k = 0.1306$ under these conditions, so that the bending moment acting on the crack is given by $M = 0.1306Ph$, and the phase angle is equal to -63.1°. The results of a finite-element calculation showing how the energy-

---

included; it is neglected throughout this paper.

release rate for a lap-shear geometry varies between the two analytical limits of Eqns. 5 and 6 are shown in Fig. 4.

If the mixed-mode fracture criterion of the adhesive layer is known, the strength of the joint can be predicted by equating the energy-release rate to the toughness at the appropriate phase angle. As an example, a simple, but general, mixed-mode failure criterion that captures the essential elements of experimental observations is given by

$$\frac{\mathcal{G}_I}{\Gamma_{Io}} + \frac{\mathcal{G}_{II}}{\Gamma_{IIo}} = 1 \tag{7}$$

where $\Gamma_{IIo}/\Gamma_{Io} = 1$ corresponds to the limit of Griffith fracture with a mode-independent toughness, and $\Gamma_{IIo}/\Gamma_{Io} = \infty$ corresponds to the limit where only the mode-I component of the energy-release rate contributes to brittle fracture. Since both the energy-release rate and the degree of mode-mixedness are functions of k, the strength of a lap-shear bond (per unit width), P_f, under conditions of linear-elastic fracture mechanics (L.E.F.M.) must be of the general form:

$$\frac{P_f}{\Gamma_{Io}} = f\left(\frac{Eh}{\Gamma_{Io}}, \frac{l}{h}, \frac{L}{l}, \frac{\Gamma_{IIo}}{\Gamma_{Io}}\right). \tag{8}$$

It is possible to use Eqns. 3, 4 and 7 to write down two asymptotic expressions for the strength of a lap-shear joint under LEFM conditions:

$$\frac{P_f}{\Gamma_{Io}} = \left\{\frac{9.33\left(\Gamma_{IIo}/\Gamma_{Io}\right)}{1.33 + \left(\Gamma_{IIo}/\Gamma_{Io}\right)}\right\}^{1/2} \left\{\frac{Eh}{\Gamma_{Io}}\right\}^{1/2} = \Lambda_1\left(\frac{\Gamma_{IIo}}{\Gamma_{Io}}\right)\sqrt{\frac{Eh}{\Gamma_{Io}}} \qquad \text{when } k = 0.50 \tag{9a}$$

$$\frac{P_f}{\Gamma_{Io}} = \left\{\frac{19.5\left(\Gamma_{IIo}/\Gamma_{Io}\right)}{3.89 + \left(\Gamma_{IIo}/\Gamma_{Io}\right)}\right\}^{1/2} \left\{\frac{Eh}{\Gamma_{Io}}\right\}^{1/2} = \Lambda_2\left(\frac{\Gamma_{IIo}}{\Gamma_{Io}}\right)\sqrt{\frac{Eh}{\Gamma_{Io}}} \qquad \text{when } k = 0.13 \tag{9b}$$

The constant of proportionality $\Lambda_1(\Gamma_{IIo}/\Gamma_{Io})$ varies between the two limits of 2.0 and 3.1 depending on the sensitivity of toughness to phase angle, whereas $\Lambda_2(\Gamma_{IIo}/\Gamma_{Io})$ varies

between 2.0 and 4.4. Equation 9a is expected to be appropriate for short stiff geometries, and the Eqn. 9b is expected to be asymptotically correct in the opposite limit of long compliant geometries with small values of Eh/Γ_{Io}. The utility of a mixed-mode linear-elastic approach such as this has been demonstrated experimentally [Fernlund and Spelt, 1991; Fernlund *et al*., 1994; Papini *et al*., 1994].

For many practical adhesives and geometries, plastic deformation of the adherends can occur before the adhesive layer fails [Kim and Kim, 1988; Lai and Dillard, 1997]. For example, beam-bending theory can be used to show that if the strength, P_f, of the lap-shear specimen is greater than

$$\frac{P_f}{\Gamma_{Io}} > \frac{1}{1+6k}\left(\frac{\sigma_Y}{E}\right)\left(\frac{Eh}{\Gamma_{Io}}\right), \qquad (10)$$

yielding will occur in the free arm of the specimen before crack growth occurs. It can be seen from Eqns. 9 and 10 that plasticity in the adherends will occur before fracture if

$$\frac{Eh}{\Gamma_{Io}} < \frac{62.0\left(\Gamma_{IIo}/\Gamma_{Io}\right)}{3.89+\left(\Gamma_{IIo}/\Gamma_{Io}\right)}\left(\sigma_Y/E\right)^{-2} \text{ to } \frac{149\left(\Gamma_{IIo}/\Gamma_{Io}\right)}{1.33+\left(\Gamma_{IIo}/\Gamma_{Io}\right)}\left(\sigma_Y/E\right)^{-2}, \qquad (11)$$

depending on the geometries and properties of the joint. If this condition is met, the strength of the joint becomes sensitive to the plastic properties of the adherends. The lack of analytical tools that can be used to provide a reliable correlation between the joint strength and the "intrinsic" properties of the adhesive layer and the adherends under these conditions has left the interpretation of single lap-shear joints in a somewhat qualitative state [Hart-Smith, 1993].

The inherent difficulties associated with plasticity can be circumvented by using cohesive-zone modeling that combines elements of both the energy- and strength-based

approaches to fracture. A mixed-mode cohesive-zone model (C.Z.M.) has been used to investigate interfacial fracture of bi-material systems [Tvergaard and Hutchinson, 1992, 1996; Wei and Hutchinson, 1997, 1999]. A similar approach has been developed and used with considerable success to model the deformation and fracture of plastically-deforming adhesive joints [Yang *et al*. 1999, 2000, 2001]. It can also be used to model the behavior of elastic joints when L.E.F.M. assumptions are violated because of large-scale deformation of the adhesive layer. The cohesive-zone model of Yang *et al*. (1999, 2000, 2001) is used in the present paper to provide an extensive examination of the behavior of single-lap shear joints in both the elastic and plastic regimes.

The results of this paper are presented in three sections. The first section is an analysis of the limit in which the adherends deform in a purely linear-elastic fashion, so that the predictions of the cohesive-zone model can be compared with the linear-elastic fracture mechanics results described earlier. This section is followed by a general analysis of geometries in which plastic and elastic deformation of the adherends can occur, so as to illustrate the general case and to explore the transition between the two modes of deformation. The results of this section are validated by making comparisons between experimental results and the predictions of associated numerical analyses using, *without modification*, a mixed-mode cohesive-zone model *previously developed for the experimental system*. The final section of this paper addresses the problem of asymmetrical lap-shear joints in which one adherend is of a different thickness from the other. Comparisons between the numerical predictions and experimental observations are again presented for this configuration.

2. Numerical approach

In this study of the lap-shear test, it is assumed that the role of the adhesive layer is to provide cohesive tractions across the interface of the joint. These tractions are dictated by the geometry, testing rate and constitutive properties of the adhesive [Yang *et al*., 1999]. Furthermore, it is assumed that the adhesive layer can fail under the influence of both shear and normal loading. Previous studies on mixed-mode failure of adhesive joints [Yang and Thouless, 2001] indicate that different cohesive laws are required for the two modes of deformation, and that two parameters are required to describe the cohesive tractions for each mode of deformation (Fig. 5). The mode-I toughness, Γ_{Io}, is the area under the mode-I traction-separation law, and the mode-I cohesive strength, $\hat{\sigma}$, is the maximum normal stress that can be supported by the adhesive layer. The mode-II toughness, Γ_{IIo}, is the area under the mode-II traction-separation law, and the mode-II cohesive strength, $\hat{\tau}$, is the maximum shear stress that can be supported by the adhesive layer. It can be shown that the precise shapes of the cohesive laws are not particularly significant.

In any mixed-mode problem, an assumption about the coupling between the two fracture modes needs to be made. The failure criterion of Eqn. 7 is particularly amenable to adaptation in a cohesive-zone analysis [Yang and Thouless, 2001]. It permits a general mode-independent failure criterion to be incorporated into the cohesive-zone model that can be used under a variety of conditions including elastic and plastic geometries. The definitions of the mode-I and mode-II components of the energy-release rates are generalized so that $\mathcal{G}_{I}$ and $\mathcal{G}_{II}$ are defined as the area under the traction-separation law integrated up to the values of the displacements dictated by the current deformation of the

joint (Fig. 5). Once the failure criterion has been met for an element in the cohesive zone, it is assumed that the element is no longer capable of bearing any load. The mode-mixedness can be deduced directly from the numerical predictions by examining the value of $\mathcal{G}_{II}/\mathcal{G}_{I}$ for a crack-tip cohesive-zone element just before it fails [Yang and Thouless, 2001], and using this ratio in the expression for the phase angle given in Eqn. 4. It should be noted that various schemes can be devised for defining mode-mixedness in these types of problem. They all tend to be affected by the cohesive properties and the mode-mixedness may vary during loading. The one proposed here appeared to be the most satisfactory way of describing mode-mixedness, and gave good agreement with the L.E.F.M. description where appropriate.

A commercial code (ABAQUS version 5.8) was used to model the adherends. Two-dimensional plane-stress elements were used for the adherends. These were assumed to exhibit linear-elastic behavior until yield and isotropic hardening after yield. A von Mises yield criterion was assumed, and the constitutive behavior of the adherends was assumed to be described by

$$\sigma = E\varepsilon \qquad \text{for } \sigma \le \sigma_Y \tag{12a}$$

$$\sigma = \sigma_Y \left(E/\sigma_Y\right)^n \varepsilon^n \qquad \text{for } \sigma \ge \sigma_Y \tag{12b}$$

where σ and ε are the uniaxial stress and strain, σ_Y is the uniaxial yield stress, E is the Young's modulus of the adherends, and n is the power-law hardening exponent. The cohesive-zone model introduces the mode-I and mode-II cohesive stresses, $\hat{\sigma}$ and $\hat{\tau}$, into the analysis, in addition to the toughness of the two modes. The strength of an equal

thickness, linear-elastic, lap-shear geometry is of the form[2]

$$\frac{P_f}{\Gamma_{Io}} = f\left(\frac{Eh}{\Gamma_{Io}}, \frac{l}{h}, \frac{L}{l}, \frac{\Gamma_{IIo}}{\Gamma_{Io}}, \frac{\hat{\sigma}}{E}, \frac{\hat{\tau}}{\hat{\sigma}}\right) \tag{13a}$$

where the first four terms are identical to the L.E.F.M. form of Eqn. 8, and the last two terms come from the parameters of the cohesive-zone model. This general form is appropriate when the adherends remain elastic, but L.E.F.M. conditions are not valid because of large-scale deformations in the adhesive. If yielding of the adherends can occur, then the additional terms σ_Y and n must be included to reflect the yield properties of the adherends:

$$\frac{P_f}{\Gamma_{Io}} = f\left(\frac{Eh}{\Gamma_{Io}}, \frac{l}{h}, \frac{L}{l}, \frac{\Gamma_{IIo}}{\Gamma_{Io}}, \frac{\hat{\sigma}}{E}, \frac{\hat{\tau}}{\hat{\sigma}}, \frac{\sigma_Y}{E}, n\right). \tag{13b}$$

In the present study, the primary emphasis is on the effects of geometry, as expressed by the first three non-dimensional groups of the equations. However, the properties of the adhesive layer (*i.e.*, $\hat{\sigma}, \hat{\tau}$, Γ_{Io} and Γ_{IIo}) are assumed to be independent of geometry. The effects of geometry on the cohesive properties of an adhesive layer have been studied by Kafkalidis *et al*. (2000), and Cavalli and Thouless (2001).

3. Results

3.1 Elastic adherends

The predictions of lap-shear strength for elastic adherends are shown in Figs. 6 to

[2] The thickness of the cohesive zone, b, and the crack length, a, are additional parameters that should be included in a full description of a mixed-mode geometry. Generally, the results are not very sensitive to the thickness of the cohesive zone if $b/h << 1$. Furthermore, calculations with non-zero values of l/h show that, for the range of cohesive strengths used in this paper, an initial crack has little influence beyond its effect on the bonded ligament length. This appears to be consistent with the observations of Papini *et al*. (1994) that the strength of adhesively-bonded lap shear joints is not strongly dependent on the existence of pre-existing cracks Therefore, unless otherwise specified, constant values of $b/h = 1/48$ and $a/h = 0$ were used for the results presented in this study.

8. Figures 6 and 7 show that the strength is very sensitive to the geometry but exhibits asymptotic steady-state behavior when both the overlap length and the total length of the specimen are long enough. In particular, Fig. 6 shows how the lap-shear strength varies as a function of overlap length. Superimposed on this plot are the limiting L.E.F.M. predictions from Eqn. 9b. These asymptotic limits are expected to be valid for relatively long compliant geometries, and it can be seen that they are in excellent agreement with the numerical results for very long overlap lengths. The mode-mixedness was also in good agreement with the L.E.F.M. predictions in this regime. However, it will also be observed from Fig. 6 that as the overlap length decreases, even the lower L.E.F.M. limit of Eqn. 9a provides a prediction that is much too large. This discrepancy arises because of large-scale deformation along the interface associated with relatively low values of the cohesive shear and normal strengths. Linear-elastic fracture-mechanics predictions are only appropriate when parameters such as $E\Gamma_{Io}/\widehat{\sigma}^2 h = \left(Eh/\Gamma_{Io}\right)^{-1}\left(\widehat{\sigma}/E\right)^{-2}$ are small, where $\widehat{\sigma}$ is a representative cohesive strength and h is a representative dimension.[3]

Figure 7 shows how the strength of a lap-shear joint varies with the total length of the specimen for a fixed overlap length. An asymptotic value is reached when the specimen length is greater than about 10 times the overlap length. In this particular example, although the overlap length is twenty times the adherend thickness it is short enough for large-scale slip to influence the strength, and the analytical results of Eqn. 9 are inappropriate. The final figure of this series (Fig. 8) shows load-displacement plots for elastic lap-shear specimens with different values of mixed-mode toughness ratio,

[3] The condition for the validity of L.E.F.M. results is usually stated as $h > 2.5(K_{Ic}/\sigma_Y^2)$, where the yield strength, σ_Y, is taken as a measure of the crack-tip cohesive strength. It can be seen that this is equivalent

Γ_{IIo}/Γ_{Io}, for fixed values of the other parameters including Eh/Γ_{Io}. The shape of the curves are all identical; the effect of increasing the mode-II toughness is to increase the strength. It should be noted that the displacement in this figure is defined as the horizontal projection of the relative displacement of two points each situated a short distance from the ends of the overlap region. Consequently, the non-linearity of the load-displacement curve close to the origin arises from rotation of the specimen upon initial loading. This rotation of the lap shear geometry needs to be considered when experimentally investigating load-displacement curves

3.2 Elastic-plastic adherends

Figures 9, 10 and 11 show how the strength depends on geometry and interfacial toughness for the general case of elastic-plastic adherends. The trends of strength with geometry are similar to the trends when the deformation is purely elastic; however, the asymptotic steady-state solutions occur at somewhat shorter specimen lengths owing to the increased deformation of the adherends. The transition between elastic and plastic behavior can be seen in Fig. 11 in which the elastic-plastic solutions are plotted as a function of Eh/Γ_{Io} for different values of yield strength. Superimposed on these plots is the purely elastic solution for identical values of the appropriate dimensionless parameters. Plasticity dominates at low values of the parameter Eh/Γ_{Io}, and elasticity dominates at higher values. The transition from plasticity to elasticity occurs at higher values of Eh/Γ_{Io} as σ_Y/E increases, as predicted by Eqn. 11. At sufficiently large values of Eh/Γ_{Io}, the deformation of the adherends is entirely elastic and the strength follows the $(Eh/\Gamma_{Io})^{1/2}$ dependence predicted by L.E.F.M. (Eqn. 9). Just below the transition,

---

to the condition $E\Gamma_{Io}/\bar{\sigma}^2 h < 0.4$

plasticity results in a lap-shear strength that increases with decreasing yield strength (Fig. 11a). It should be noted that if the ratio $\widehat{\sigma}/\sigma_Y$ was significantly higher than the values chosen for this study, the solutions at large values of Eh/Γ_{Io} would tend to a small-scale yielding limit, in which crack-tip plasticity would result in a higher effective toughness [Tvergaard and Hutchinson, 1992], rather than the elastic limit shown in Fig. 11a.

Somewhat surprisingly, the trends described above are reversed at very low values of Eh/Γ_{Io}, and the lap-shear strength increases with increasing yield strength (Fig. 11b). This behavior is geometrical in origin and is coupled to the fact that Γ_{IIo} is much larger than Γ_{Io}. As Eh/Γ_{Io} is reduced, the critical normal displacement for fracture increases, eventually reaching values which are too large to be accommodated by the smoothly curved elastic substrates. Consequently, failure will occur only with a significantly increased contribution from mode-II deformation, thereby increasing the strength. This increase in strength is accompanied by an increase in the magnitude of the phase angle at fracture from about 65° (as predicted by L.E.F.M.) to 80° or more. On the other hand, plastic joints can form plastic hinges near the roots of the overlap regions and accommodate large local deformations. The resulting "peel" type of failure means that the mode-I component becomes more dominant when the yield strength of the adherends drops and, consequently, the strength drops with yield strength.

3.3 Comparisons between experimental and numerical results

The numerical results presented in this paper were tested by comparing them to experimental observations using a bonded system for which the mixed-mode fracture

parameters have been well-characterized in earlier work [Yang and Thouless, 2001]. In this earlier work, it was shown that both the form of the load-displacement curves and the deformation could be accurately predicted. These comparisons were confined to a limited set of similar geometries with different adherend thicknesses. In the present study, the comparison was extended to look at the effects of overlap length and the effects of asymmetry in the adherend thickness. The symmetrical single-lap-shear specimens were made from 2.0 mm thick 5754 aluminum alloy sheets bonded using a commercial adhesive (Ciba Specialty Chemicals XD4600) with a bond-line thickness of 250 μm. The thickness of the adhesive layer was maintained by using uniform glass spheres as spacers. Teflon® tape was used to limit the extent of the adhesive to the overlap region. The details of the bonding process is outlined elsewhere [Thouless *et al.*, 1998]. A series of tests were conducted to measure the lap-shear strength of these joints using different overlaps ranging from 2 mm (l/h = 1) to 50 mm (l/h = 25), with the overall length of the joints being maintained at L = 300 mm. The velocity of the ends of the specimens was kept constant at 0.2 mm.s^{-1}. The displacement was measured optically using two points separated by a gauge length of 75 mm. At the magnification used, these measurements had a spatial resolution of ± 40 μm. The numerical calculations were conducted using, *without modification*, the mixed-mode fracture parameters previously established for this system. The mode-I values (for interfacial fracture, as is appropriate for the mixed-mode loading in a lap-shear test) were Γ_{Io} = 1.0 ± 0.15 kJm^{-2} and $\widehat{\sigma}$ = 60 ± 10 MPa, and the mode-II values were Γ_{IIo} = 5.4 ± 0.8 kJm^{-2} and $\widehat{\tau}$ = 35 ± 5 MPa [Yang and Thouless, 2001]. As determined from uniaxial tensile tests, the modulus and yield strength of the aluminum were taken to be 69 GPa and 95 MPa, while the power-

law hardening exponent, n was taken to be 0.238. The agreements between the results of the numerical calculations and the experimental behavior of the joints with different overlap lengths were generally excellent. As with the earlier results of Yang and Thouless [2001], fairly accurate predictions for the loads, displacements and deformations were obtained. For example, a summary of the experimental and numerical results for the dependence of lap-shear strength on overlap length is given in Fig. 12. It should be noted that, as discussed earlier, the behavior of the lap-shear geometry is very sensitive to boundary conditions, and the experimental configuration results in a slight rotation and, hence, slight misalignment of the grips. This effect was not mimicked numerically, and may be responsible for the slight discrepancies in the predicted strengths that can be seen in Fig. 12.

To complete this work on lap-shear geometries, a second series of experiments and simulations were done using asymmetrical single lap-shear joints (Fig. 1b) for which the ratio between the adherend thicknesses provides an additional dimensionless group that affects the strength of the joint. These specimens were fabricated in an identical fashion to the symmetrical set. The length of the bonded segments, l, was kept at 25 mm, the overall length of the specimens, L, was kept at 180 mm, and the gauge length for the displacement measurements was 55 mm for all specimens. The adhesive thickness was 250 μm, and the thicknesses of the adherends was varied between 1.0 mm and 3.0 mm, giving a range of thickness ratios, h_1:h_2, of between 3.0 and 1.0. Since the two arms were of unequal thickness, square shims of complementary thickness were bonded to the ends of each free arm, so that the joints would not be artificially rotated when clamped in the aligned machine grips. During the test, the arms of the specimens were pulled apart by a

tensile testing machine at a constant displacement rate of 0.2 mm.s^{-1}. A high-resolution C.C.D. camera was used to observe the deformation, and the crack initiation and propagation. In all cases, except for the h_1:h_2 = (3.0 mm):(2.3 mm) combination, a stable crack was initiated at the interface between the adhesive and the thinner arm and propagated roughly halfway along the overlap before the onset of an instability led to very fast fracture. The h_1:h_2 = (3.0 mm):(2.3 mm) specimens exhibited an instability as soon as the initial crack was formed. A sequence of four images for a typical example of stable crack growth with h_1:h_2 = (2.0 mm):(1.0 mm) is shown in Fig. 13. It will be observed that the crack propagation is reminiscent of crack growth in a peel test. The thinner arm peels off the thicker one, with a plastic hinge forming at the root of the thin arm and moving along the bonded region.

Using the same parameters for the cohesive-zone and aluminum described above, numerical predictions were made for the deformation and load-displacement curves. These were all in good agreement with the experimental observations. For example, the predictions for the deformed shapes of a specimen with h_1:h_2 = (2.0 mm):(1.0 mm) at various stages during a test are shown in Fig. 14, and can be compared with the experimentally observed shapes illustrated in Fig. 13. Figures 15a and 15b show comparisons between the numerical predictions for the load-displacement curves and the experimentally observed curves for thickness ratios of h_1:h_2 = (3.0 mm):(2.3 mm) and h_1:h_2 = (2.0 mm):(1.0 mm). In particular, it should be noted that the numerical results predicted the much higher loads and lower displacements for the thickness ratio of h_1:h_2 = (3.0 mm):(2.3 mm). The onset of crack growth is indicated for both the experimental and numerical curves. Both the experimental results and the numerical

predictions show an instability occurring at the onset of crack growth for a thickness ratio of h_1:h_2 = (3.0 mm):(2.3 mm), but a regime of stable crack growth for a thickness ratio of h_1:h_2 = (1.0 mm):(2.0 mm). The peak load in these figures, which corresponds to crack initiation, depends strongly on the thickness of the adherends. Similar agreements were obtained for all the other thickness ratios that were studied.

4. Conclusions

The mechanics of the lap-shear geometry can be quite complicated, even under conditions when linear-elastic fracture mechanics (L.E.F.M.) are appropriate, owing to a great sensitivity to geometrical parameters. When the cohesive strength of the adhesive is low enough for large-scale deformations within the interfacial layer to become important, or when non-linear deformations occur within the adherend, a numerical cohesive-zone approach combining strength and energy considerations is required to describe the behavior. The results of such a model have been presented in this paper. In the first part of the paper, the results for adherends that remain elastic have been presented. Provided the effects of large-scale deformations (caused by both shear and normal tractions across the interface) are limited, L.E.F.M. results provide a reasonable approximation to the fracture behavior. The effects of plastic deformation in the adherends become important at low values of Eh/Γ_{Io} and σ_Y/E; *i.e.*, when the toughness of the interface is high, the thickness of the adherends is low, or if the yield stress of the adherends is low. Plasticity in the adherends occurs below a critical value of Eh/Γ_{Io}, and just below this transition the lap-shear strength increases with a decrease in yield strength, However, at much lower values of Eh/Γ_{Io}, plasticity tends to reduce the lap-shear strength because it enhances local peeling deformations and increases the effect of

mode-I failure. Very large cohesive stresses may also introduce crack-tip plasticity in the adherends, but these effects have not been explored for the adhesive-joint applications considered here. The final portion of this paper compares the numerical predictions with experimental observations. A commercial adhesive / aluminum adherend system was used for which the cohesive-zone parameters had been determined in earlier work. These parameters were used directly in the numerical modeling with no modification at all. The resulting predictions showed excellent agreement with the experimental observations.

Acknowledgements

This work was partially supported by NSF Grant CMS-9624452. The support and help of Dr. Susan Ward and Dr. John Hill of the Ford Motor Company, and of Dr. Qingda Yang are particularly appreciated.

References

Adams, R. D. and Peppiatt, N. A., (1974). "Stress Analysis of Adhesively-Bonded Lap Joints," *Journal of Strain Analysis*, **9**, 185-196.

Allman, D. J., (1977). "A Theory for Elastic Stresses in Adhesive Bonded Lap Joints," *Quarterly Journal of Mechanics and Applied Mathematics*, **30**, 415-436.

Anderson, G. P., Brinton, S. H., Ninow, K. J., and DeVries, K. L. (1988). "A Fracture Mechanics Approach to Predicting Bond Strength," in *Advances in Adhesively-Bonded Joints*, ASME, New York, 93-101.

Bigwood, D. A. and Crocombe, A. D., (1989). "Elastic Analysis and Engineering Design Formulae for Bonded Joints," *International Journal of Adhesion and Adhesives*, **9**, 229-242.

Bigwood, D. A. and Crocombe, A. D., (1990). "Non-Linear Adhesive Bonded Joint Design Analyses," *International Journal of Adhesion and Adhesives*, **10**, 31-41.

Cavalli, M. N. and Thouless, M. D., (2001). "The Effect of Damage Nucleation on the Toughness of an Adhesive Joint," *J. Adhesion*, **76**, 75-92.

Chai, H., (1988). "Shear fracture," *International Journal of Fracture*, **37**, 137-159.

Chen, D. and Cheng, S., (1983). "An Analysis of Adhesive-Bonded Single-Lap Joints," *Journal of Applied Mechanics*, **50**, 109-115.

Crocombe, A. D. and Bigwood, D. A., (1992). "Development of a Full Elasto-Plastic Adhesive Joint Design," *Journal of Strain Analysis for Engineering Design*, 27, 211-218.

Fernlund, G. and Spelt, J. K., (1991). "Analytical Method for Calculating Adhesive Joint Fracture Parameters," *Engineering Fracture Mechanics*, **40**, 119-132.

Fernlund, G., Papini, M., McCammond, D. and Spelt, J. K., (1994). "Fracture Load Predictions for Adhesive Joints," *Composite Science and Technology*, **51**, 587-600.

Goland, M. and Reissner, E., (1944). "The Stress in Cemented Joints," *Journal of Applied Mechanics*, **66**, A17-A27.

Harris, J. A. and Adams, R. D., (1984). "Strength Prediction of Bonded Single Lap Joints by Non-linear Finite Element Methods," *International Journal of Adhesion and Adhesives*, **4,** 65-78.

Hart-Smith, L. J., (1973). "Adhesive-Bonded Single-Lap Joints," *NASA Technical Report* CR-112236.

Hart-Smith, L. J., (1993). "Bonded Lap-Shear Test Coupon - Useful for Quality Assurance but Dangerously Misleading for Design Data," pp. 239-246 in *Proceedings of the 1993 38th International SAMPE Symposium and Exhibition*, *(Advanced Materials: Performance Through Technology),* Anaheim, CA, USA.

Kafkalidis, M. S., Thouless, M. D., Yang, Q. D. and Ward, S. M., (2000). "Deformation and Fracture of an Adhesive Layer Constrained by Plastically-deforming Adherends," *J. Adhes. Sci. Technol.* **14**, 1593-1607.

Kim, K. S. and Kim, J., (1988). "Elasto-Plastic Analysis of the Peel Test for Thin Film Adhesion," *Journal of Engineering Materials and Technology*, **110**, 266-273.

Lai, Y.-H., Rakestraw, M. D. and Dillard, D. A., (1996). "The Cracked Lap Shear Specimen Revisited - A Closed Form Solution," *International Journal of Solids and Structures,* **33**, 1725-1743.

Lai, Y.-H. and Dillard, D. A., (1997). "Using the Fracture Efficiency to Compare Adhesion Tests," *International Journal of Solids and Structures,* **34**, 509-525).

Papini, M., Fernlund, G. and Spelt, J.K., (1994). "The Effect of Geometry on the Fracture of Adhesive Joints," *International Journal of Adhesion and Adhesives,* **14**, 5-13.

Suo, Z. and Hutchinson, J.W., (1990). "Interface Crack Between Two Elastic Layers," *International Journal of Fracture,* **43**, 1-18.

Tong, L., (1996). "Bond Strength for Adhesive Bonded Single Lap Joints," *Acta Mechanica*, **117**, 103-113.

Tsai, M. Y. and Morton, J., (1994). "An Evaluation of Analytical and Numerical Solutions to the Single-Lap Joint," *International Journal of Solids and Structures*, **31**, 2537-2563.

Tsai, M. Y. and Morton, J., (1995). "An Experimental Investigation of Non-Linear Deformations in Single-Lap Joints," *Mechanics of Materials*, **20**, 183-194.

Tsai, M. Y., Oplinger, D. W., and Morton, J., (1998). "Improved Theoretical Solutions for Adhesive Lap Joints," *International Journal of Solids and Structures*, **35**, 1163-1185.

Tvergaard, V. and Hutchinson, J. W., (1992). "The Relation between Crack Growth Resistance and Fracture Process Parameters in Elastic-Plastic Solids, *Journal of the Mechanics and Physics of Solids*, **40**, 1377-1397.

Tvergaard, V. and Hutchinson, J. W., (1996). "Toughness of Ductile Adhesive Joints," *Journal of the Mechanics and Physics of Solids*, 789-800.

Wei, Y. and Hutchinson, J. W., (1997). "Nonlinear Delamination Mechanics for Thin Films," *Journal of the Mechanics and Physics of Solids*, **45,** 1137-1159.

Wei, Y. and Hutchinson, J. W., (1999). "Interface Strength, Work of Adhesion and Plasticity in the Peel Test," *International Journal of Fracture*, **93,** 315-333.

Yang, Q. D., Thouless, M. D. and Ward, S. M., (1999). "Numerical Simulations of Adhesively-Bonded Beams Failing with Extensive Plastic Deformation," *Journal of the Mechanics and Physics of Solids*, **47**, 1337-1353.

Yang, Q. D., Thouless, M. D. and Ward, S. M., (2000). "Analysis of the Symmetrical 90^0-Peel Test with Extensive Plastic Deformation," *Journal of Adhesion*, **72**, 115-132.

Yang, Q. D., Thouless, M. D., (2001). "Mixed-Mode Fracture Analyses of Plastically-Deforming Adhesive Joints," *International Journal of Fracture***, 110**, 175-187.

Figure captions

Figure 1 **(a)** Single lap-shear geometry. **(b)** Asymmetrical lap-shear geometry.

Figure 2 Load and moments acting on a symmetrical, single-lap-shear specimen.

Figure 3 Configuration and distribution of loads and moments at the **(a)** low-load, or stiff, limit for a single-lap-shear joint, and **(b)** high-load, or compliant, limit for a single-lap-shear joint.

Figure 4 The variation of energy-release rate with load under plane-stress linear-elastic fracture-mechanics conditions for a single-lap-shear joint. For these calculations, $l/h = 60$, $L/l = 16.5$, and a crack of length $a/h = 10$ extended from each side of the bonded region. The ends of the specimen were prevented from rotating.

Figure 5 Schematic illustrations of the mode-I and mode-II traction-separation laws used for the mixed-mode cohesive-zone calculations.

Figure 6 Plot of normalized strength versus normalized overlap length for elastic, single-lap-shear joints. The other dimensionless parameters for this figure are $L/l = 11$, $\widehat{\sigma}/E = 8.7\text{x}10^{-4}$, $\widehat{\tau}/\widehat{\sigma} = 0.58$ and $\Gamma_{IIo}/\Gamma_{Io} = 5.4$..

Figure 7 Plot of normalized strength versus normalized total length for elastic, single-lap-shear joints. The other dimensionless parameters for this figure are $l/h = 20$, $\widehat{\sigma}/E = 8.7\text{x}10^{-4}$, $\widehat{\tau}/\widehat{\sigma} = 0.58$ and $\Gamma_{IIo}/\Gamma_{Io} = 5.4$.

Figure 8 Plots of load *versus* displacement for elastic, single-lap-shear joints with different values of Γ_{IIo}/Γ_{Io}. The other dimensionless parameters for this figure are $L/l = 11$, $l/h = 100$, $\hat{\sigma}/E = 1.0 \times 10^{-3}$ and $\hat{\tau}/\hat{\sigma} = 0.58$. The three different loading curves superimpose upon one another. The displacement for this plot is defined as the projection along the axis of the specimen of the displacement of two gauge points located on the centroidal axes of the arms at a distance $L_g = 108h$ apart. Therefore, the non-linearity at the origin of the curve arises from this definition of displacement and from the initial rotation of the specimen.

Figure 9 Plot of normalized strength versus normalized overlap length for elastic-plastic lap-shear joints. The other dimensionless parameters for this figure are $L/l = 11$, $\hat{\sigma}/E = 8.7\text{x}10^{-4}$, $\hat{\tau}/\hat{\sigma} = 0.58$, $\Gamma_{IIo}/\Gamma_{Io} = 5.4$, $\hat{\sigma}/\sigma_Y = 0.75$ and $n = 0.238$.

Figure 10 Plot of normalized strength versus normalized total length for elastic-plastic lap-shear joints. The other dimensionless parameters for this figure are $l/h = 20$, $\hat{\sigma}/E = 8.7\text{x}10^{-4}$, $\hat{\tau}/\hat{\sigma} = 0.58$, $\Gamma_{IIo}/\Gamma_{Io} = 5.4$, $\hat{\sigma}/\sigma_Y = 0.75$ and $n = 0.238$.

Figure 11 Plots of normalized strength versus Eh/Γ_{Io} for elastic-plastic lap-shear joints for different values of σ_Y/E. The dimensionless parameters for this figure are $L/l = 11$, $l/h = 100$, $\hat{\sigma}/E = 10^{-3}$, $\hat{\tau}/\hat{\sigma} = 0.58$, $\Gamma_{IIo}/\Gamma_{Io} = 5.0$ and $n = 0.238$. **(a)** Shows the behavior over a wide range of values for Eh/Γ_{Io}. **(b)** Shows the behavior at the higher end of the range. Superimposed on

both of these plots are the numerical predictions for the strength of a perfectly elastic lap-shear joint with the same cohesive-zone and geometrical parameters.

Figure 12 A comparison between the measured and numerically-predicted peak loads for a series of symmetrical lap-shear joints made with 2.0 mm thick aluminum adherends bonded with a 250 μm thick layer of a commercial adhesive (Ciba Specialty Chemicals XD4600). There was no initial crack in either the numerical simulations or in the experimental configuration. However, Teflon® tape was used to prevent the adhesive from bonding outside the overlap region.

Figure 13 A sequence of images showing the propagation of a stable crack in a lap-shear geometry with h_1:h_2 = (2.0 mm):(1.0 mm). **(a)** The initial state of the specimen. **(b)** An advanced state of plastic deformation of the thinner arm prior to crack initiation. A plastic hinge has formed near the overlap area. **(c)** Initial stage of crack growth, which occurs after the thinner arm has been drawn significantly. **(d)** A steady-state crack, advancing as the plastic hinge formed by the thinner arm moves along the interface of the adhesive layer.

Figure 14 Images showing the numerical predictions for the sequence of deformation and crack growth in an asymmetric, single, shear-lap joint that has a thickness ratio of h_1:h_2 = (2.0mm:1.0 mm). The parameters used in these calculations were appropriate for the experimental system of Figure 13.

Figure 15 The load-displacement curve for asymmetrical lap-shear joints with **(a)** a thickness ratio of h_1:h_2 = (2.0 mm):(1.0 mm) and **(b)** a thickness ratio of h_1:h_2 = (3.0 mm):(2.3 mm). The displacement is defined as the projection along the axis of the specimen of the displacement of two gauge points located 55 mm apart on the centroidal axes of the arms. There was no initial crack in either the numerical simulations or in the experimental configuration; Teflon® tape was used to prevent the adhesive from bonding outside the overlap region.

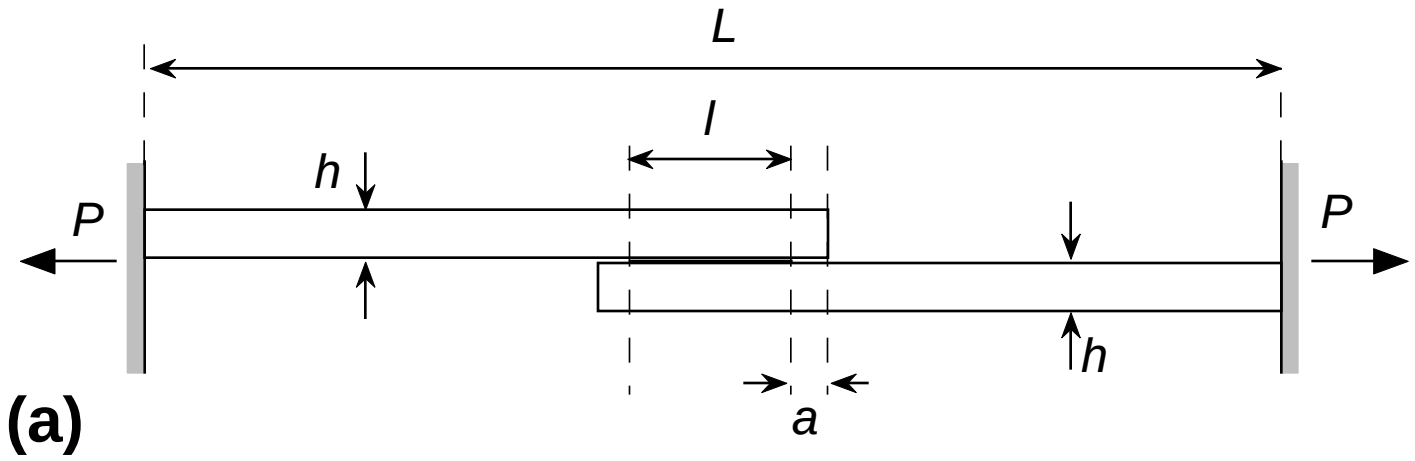

(a)

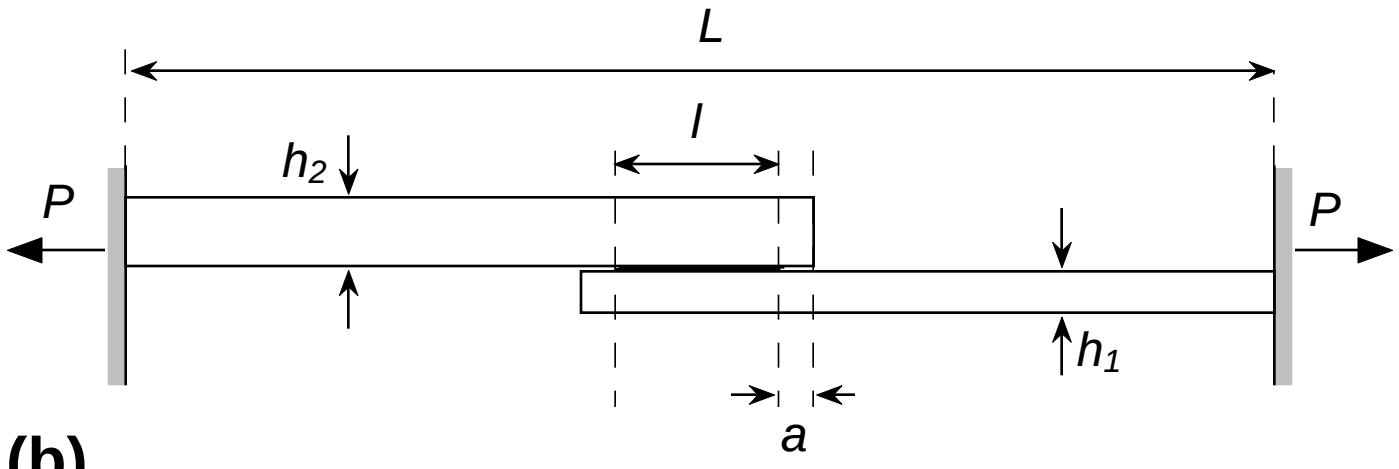

(b)

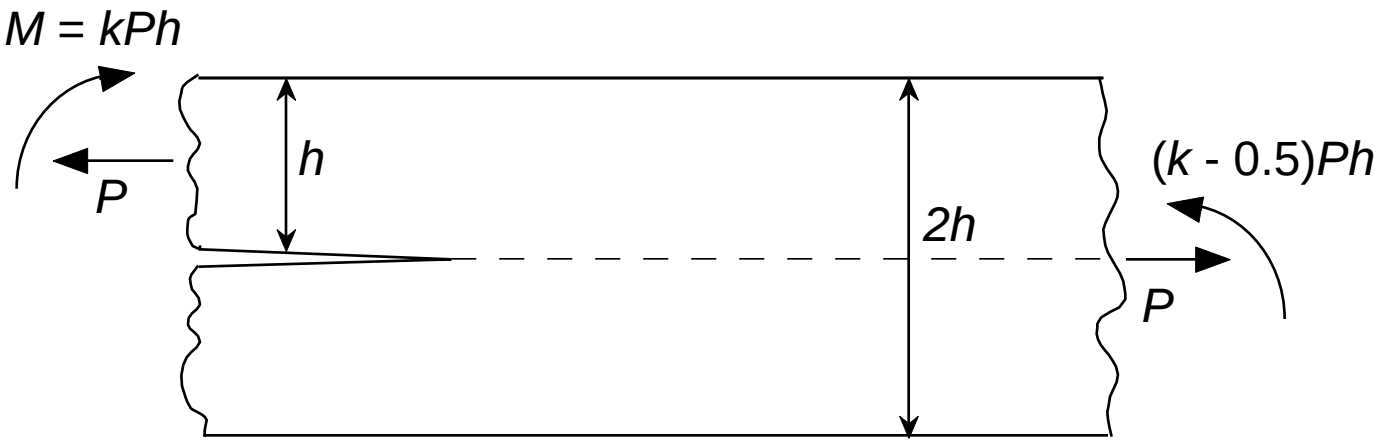
M = kPh
h
P
2h
(k - 0.5)Ph
P

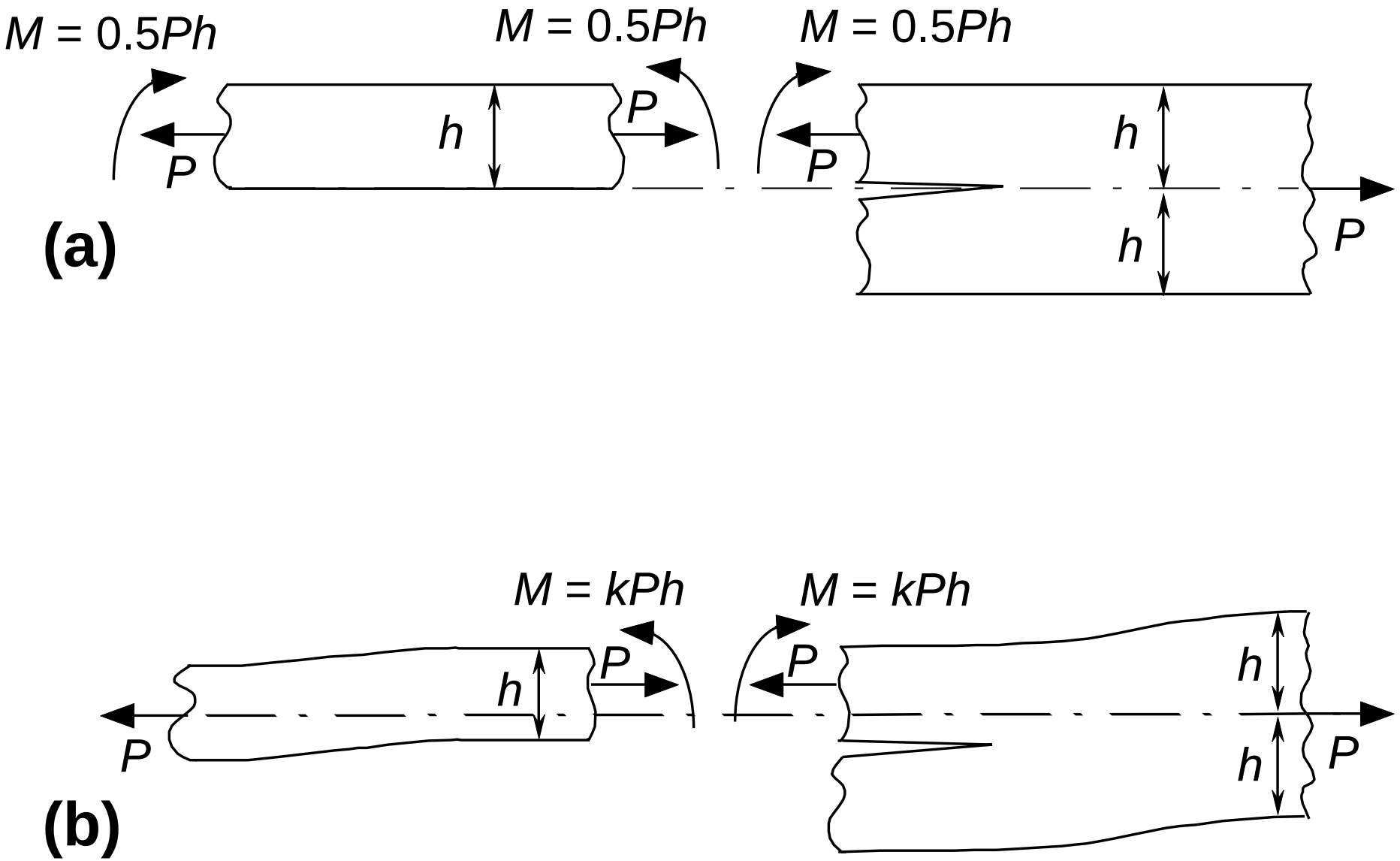
M = 0.5Ph
M = 0.5Ph
M = 0.5Ph
h
P
P
h
P
h
P
(a)
M = kPh
M = kPh
h
P
P
h
P
h
P
(b)

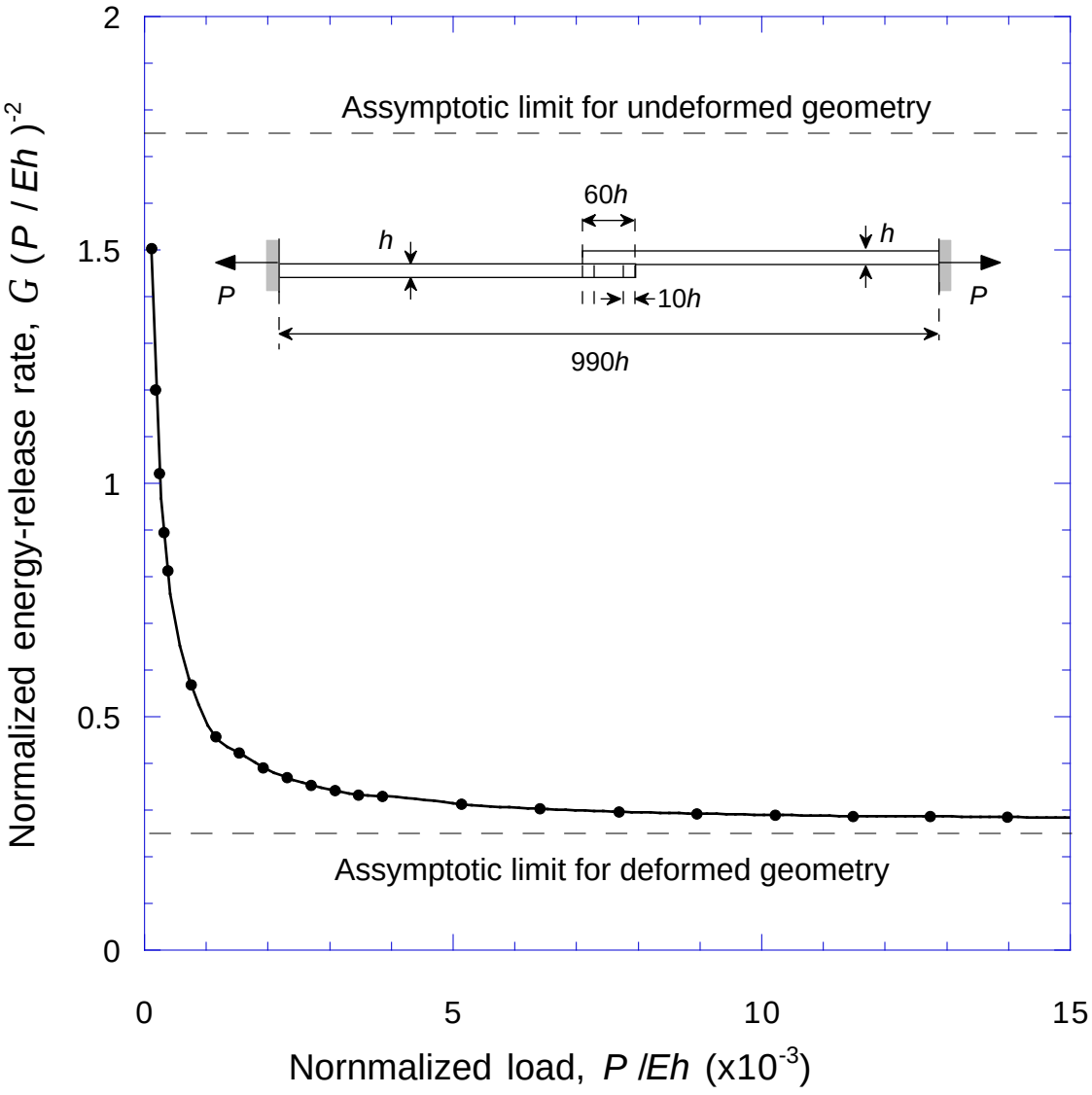
Assymptotic limit for undeformed geometry
Assymptotic limit for deformed geometry
60h
h
h
10h
990h
P
P
Normalized energy-release rate, G (P / Eh)-2
Nornmalized load, P /Eh (x10-3)
0
0.5
1
1.5
2
0
5
10
15

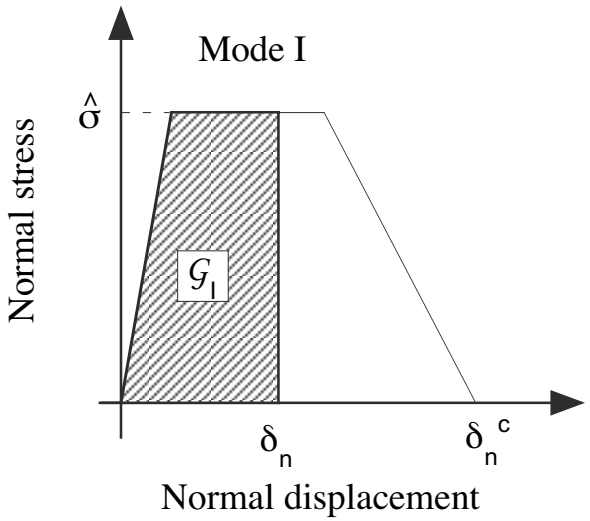
Mode I
$\hat{\sigma}$
$\mathcal{G}_I$
Normal stress
δ_n
δ_n^c
Normal displacement

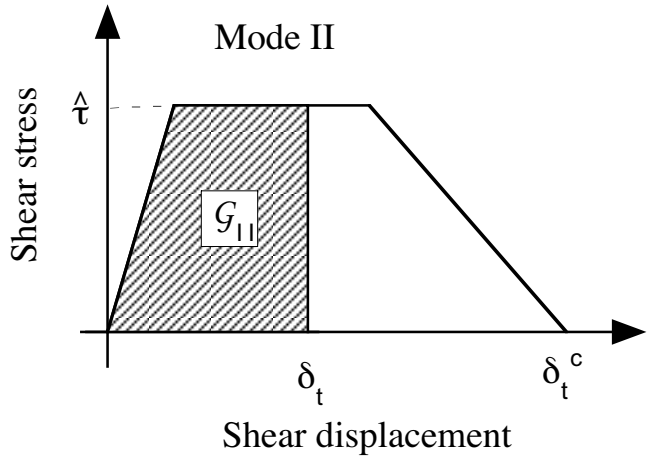
Mode II
$\hat{\tau}$
$\mathcal{G}_{II}$
Shear stress
δ_t
δ_t^c
Shear displacement

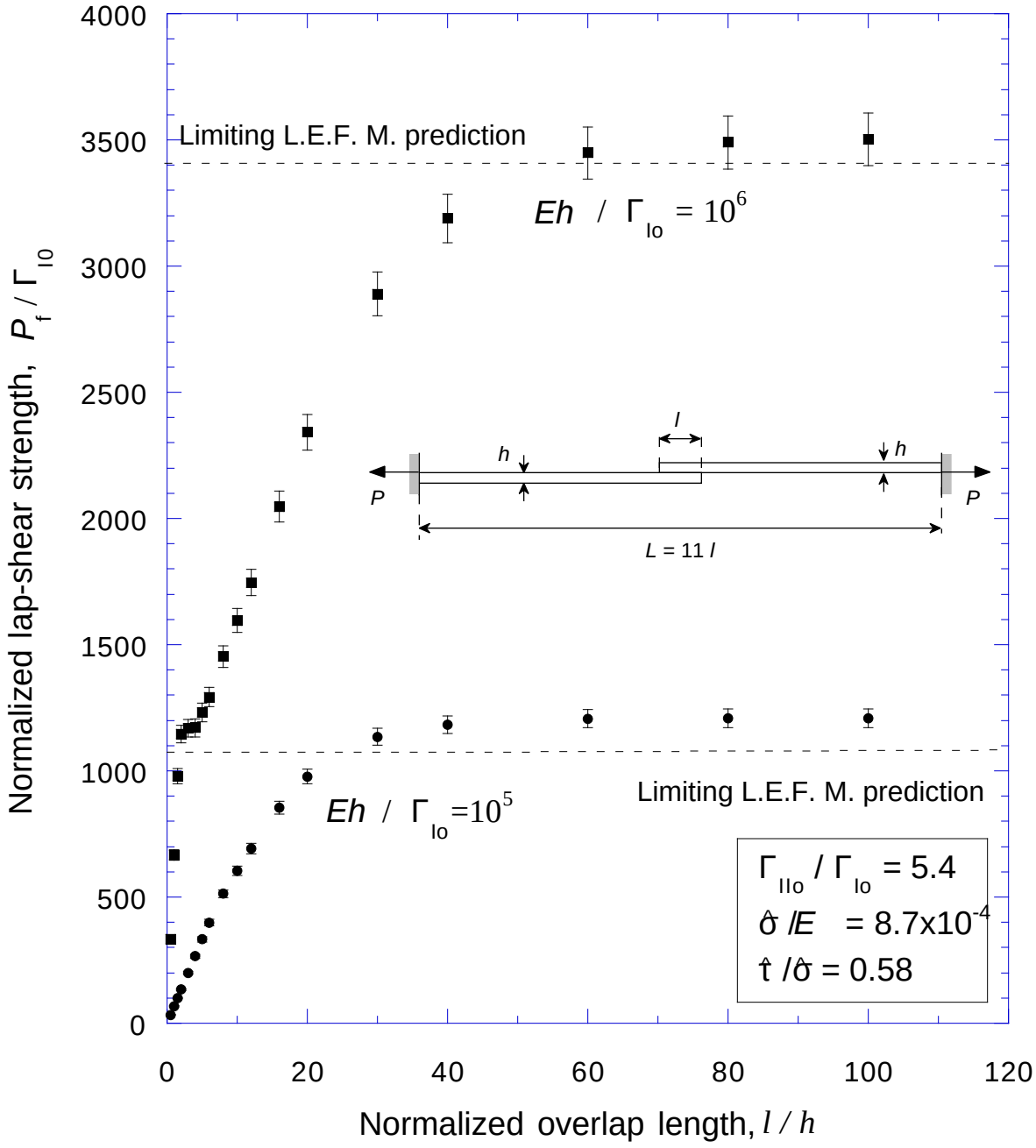
Limiting L.E.F. M. prediction
Eh / Γ_Io = 10^6
Limiting L.E.F. M. prediction
Eh / Γ_Io=10^5
Γ_IIo / Γ_Io = 5.4
σ̂ /E = 8.7x10^-4
t̂ /σ̂ = 0.58
h
l
h
P
P
L = 11 l
Normalized lap-shear strength, P_f / Γ_I0
Normalized overlap length, l / h
0
500
1000
1500
2000
2500
3000
3500
4000
0
20
40
60
80
100
120

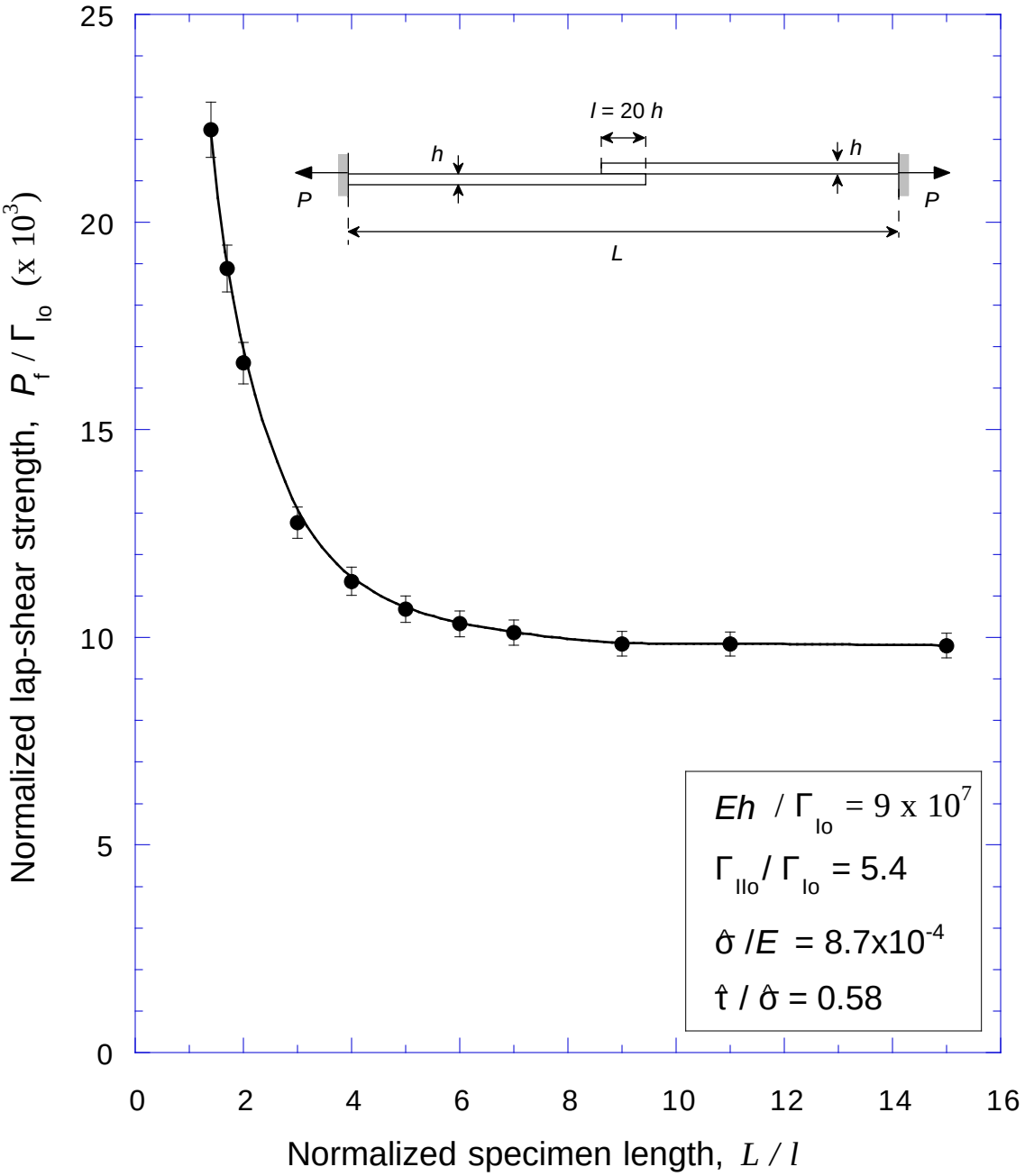
Normalized lap-shear strength, P_f / Γ_{Io} (x 10^3)
Normalized specimen length, L / l
l = 20 h
h
h
P
P
L
Eh / Γ_{Io} = 9 x 10^7
$\Gamma_{IIo} / \Gamma_{Io}$ = 5.4
$\hat{\sigma} / E$ = 8.7x10^{-4}
$\hat{\tau} / \hat{\sigma}$ = 0.58
0
5
10
15
20
25
0
2
4
6
8
10
12
14
16

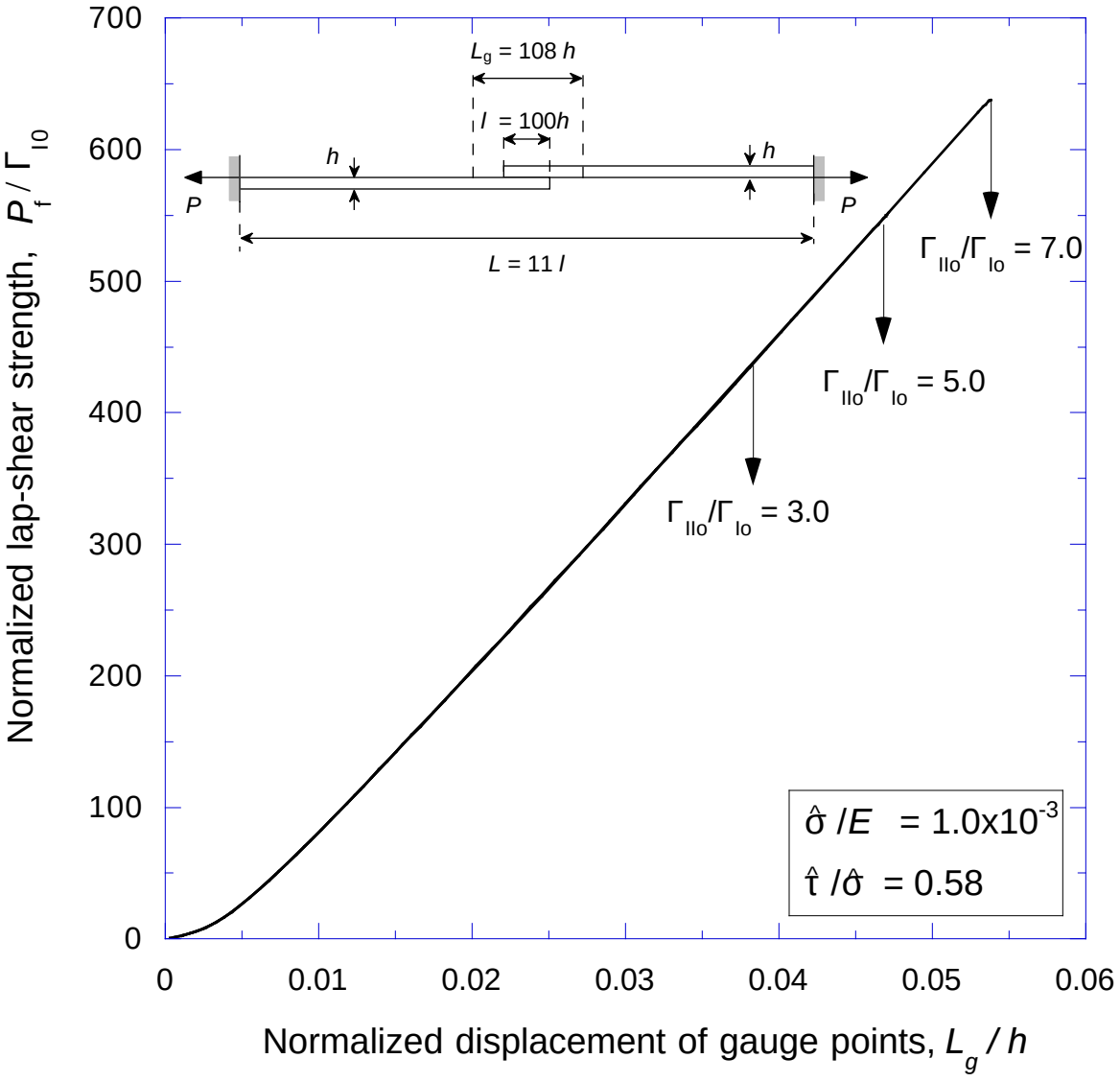
700
600
500
400
300
200
100
0
0
0.01
0.02
0.03
0.04
0.05
0.06
Normalized lap-shear strength, P_f / Γ_{I0}
Normalized displacement of gauge points, L_g / h
L_g = 108 h
l = 100h
h
h
P
P
L = 11 l
Γ_{IIo}/Γ_{Io} = 7.0
Γ_{IIo}/Γ_{Io} = 5.0
Γ_{IIo}/Γ_{Io} = 3.0
$\hat{\sigma} / E$ = 1.0x10^{-3}
$\hat{\tau} / \hat{\sigma}$ = 0.58

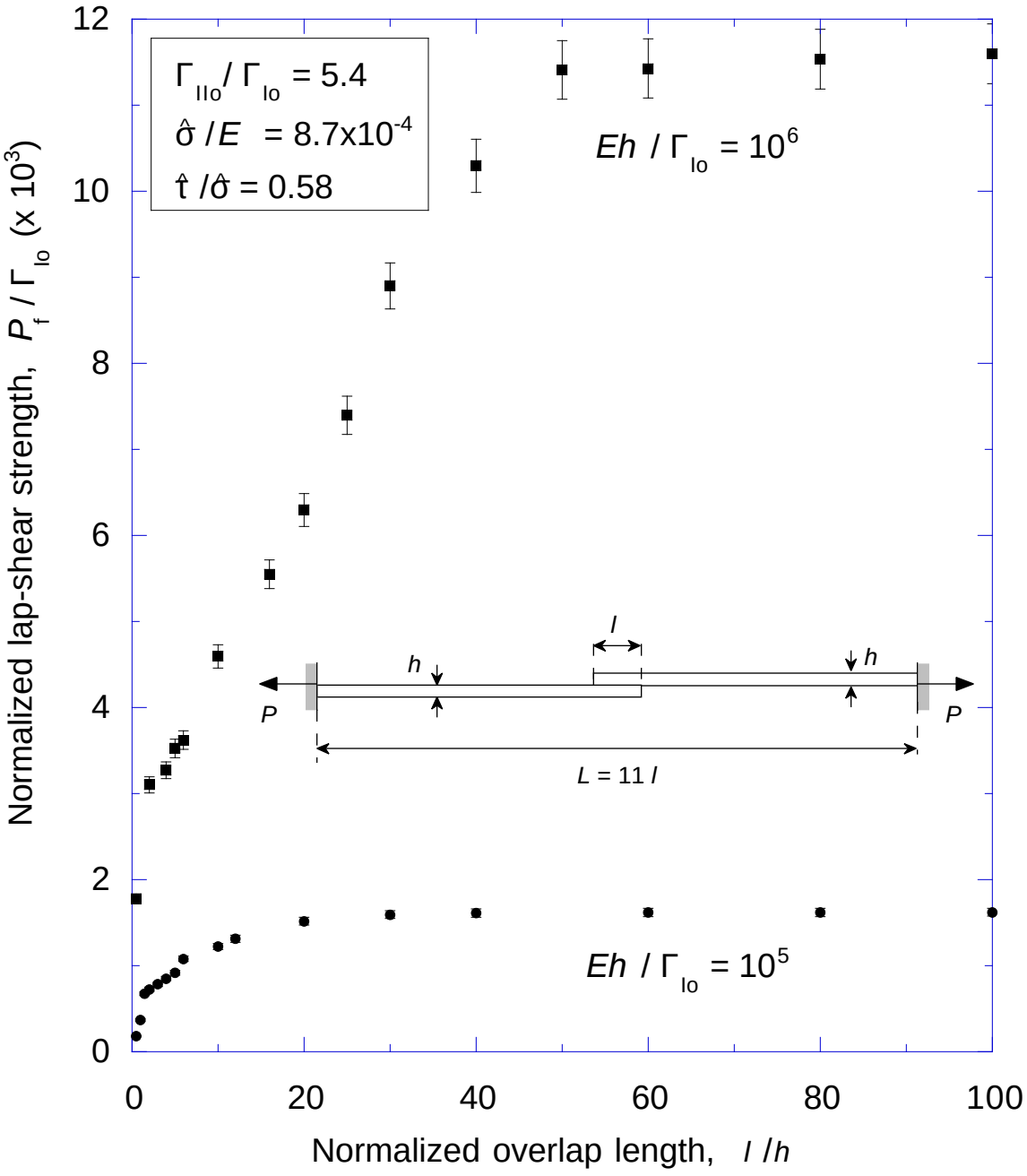
Γ_IIo / Γ_Io = 5.4
σ̂ / E = 8.7x10^-4
τ̂ / σ̂ = 0.58
Eh / Γ_Io = 10^6
Eh / Γ_Io = 10^5
h
l
h
P
P
L = 11 l
Normalized lap-shear strength, P_f / Γ_Io (x 10^3)
Normalized overlap length, l / h
0
2
4
6
8
10
12
0
20
40
60
80
100

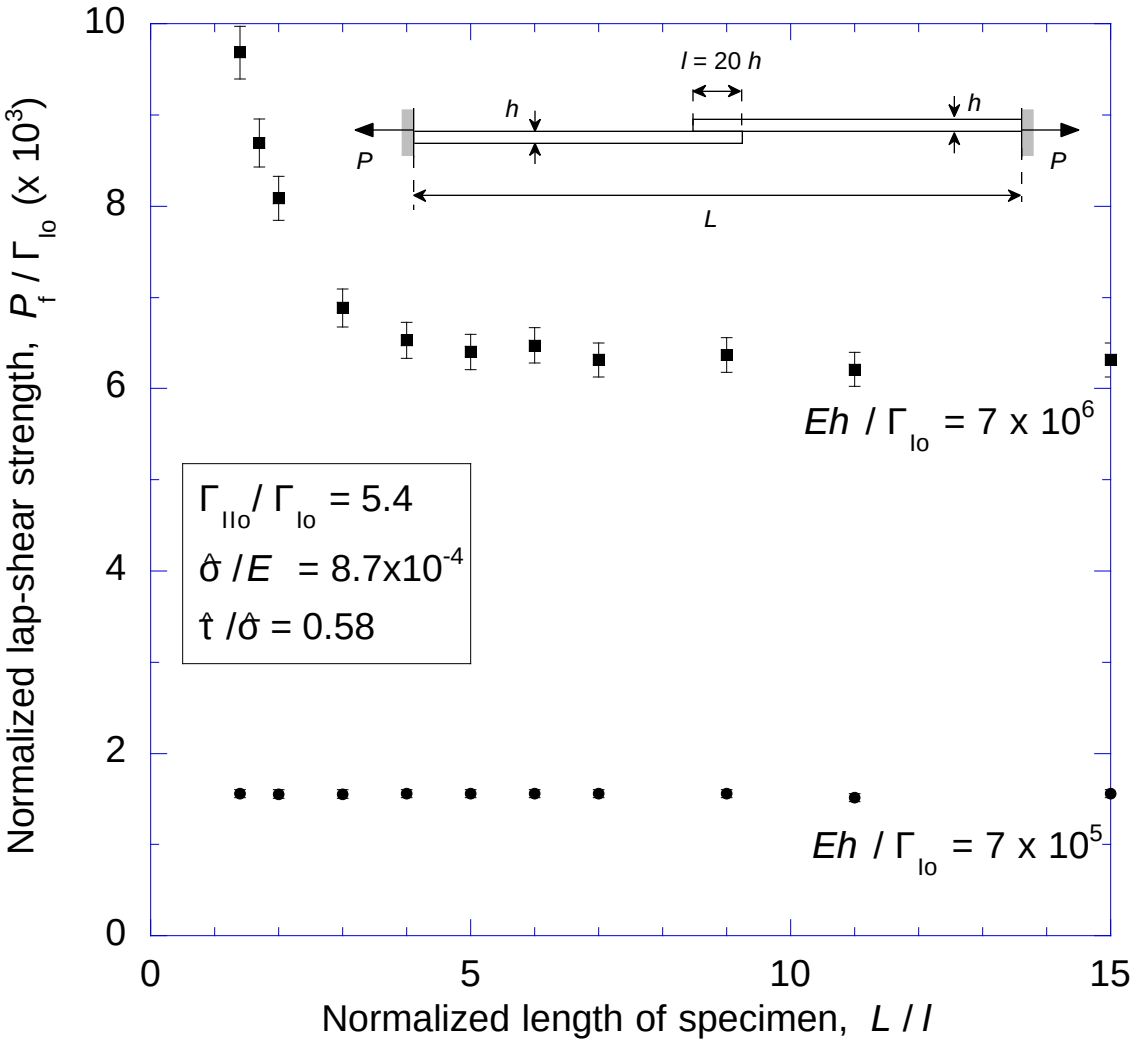
Normalized lap-shear strength, P_f / Γ_{Io} (x 10^3)
Normalized length of specimen, L / l
l = 20 h
h
h
P
P
L
Eh / Γ_{Io} = 7 x 10^6
Eh / Γ_{Io} = 7 x 10^5
$\Gamma_{IIo} / \Gamma_{Io}$ = 5.4
$\hat{\sigma} / E$ = 8.7x10^{-4}
$\hat{\tau} / \hat{\sigma}$ = 0.58
0
2
4
6
8
10
0
5
10
15

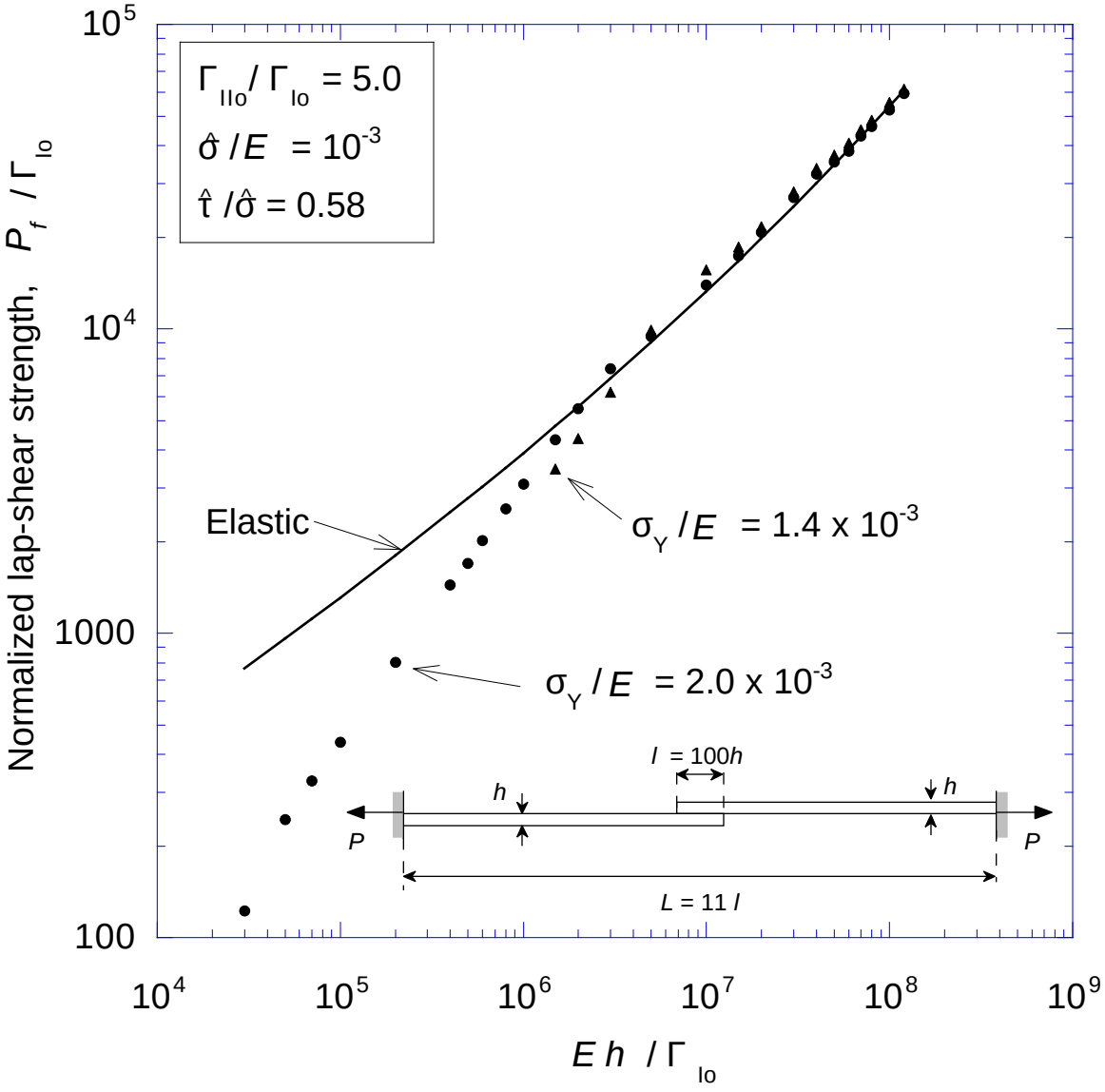
Γ IIo / Γ Io = 5.0
σ̂ / E = 10^-3
τ̂ / σ̂ = 0.58
Elastic
σ_Y / E = 1.4 x 10^-3
σ_Y / E = 2.0 x 10^-3
l = 100h
h
h
P
P
L = 11 l
Normalized lap-shear strength, P_f / Γ Io
E h / Γ Io
10^5
10^4
1000
100
10^4
10^5
10^6
10^7
10^8
10^9

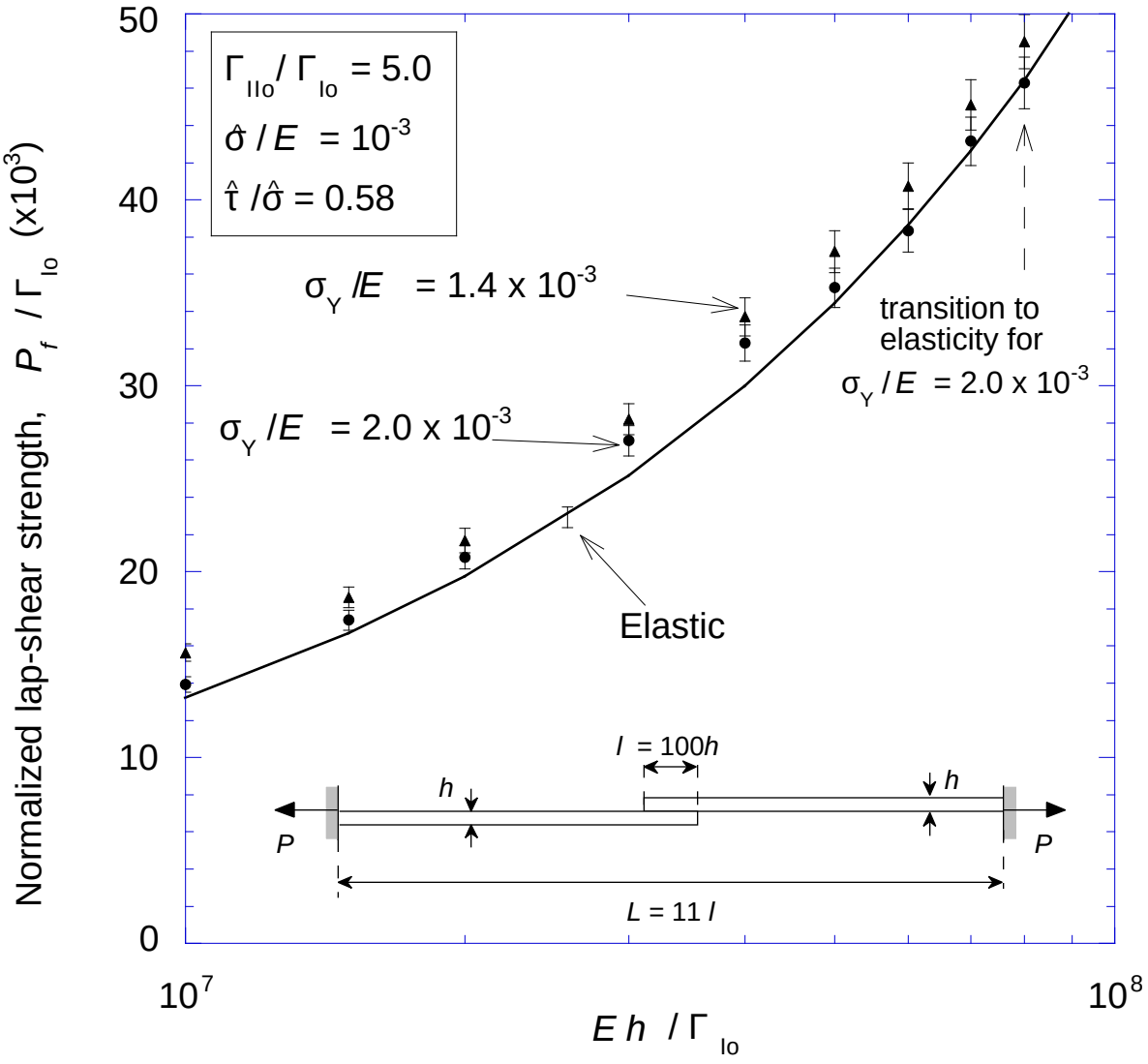
Γ IIo / Γ Io = 5.0
σ̂ / E = 10^-3
τ̂ /σ̂ = 0.58
σY /E = 1.4 x 10^-3
σY /E = 2.0 x 10^-3
transition to elasticity for
σY / E = 2.0 x 10^-3
Elastic
l = 100h
h
h
P
P
L = 11 l
Normalized lap-shear strength, Pf / Γ Io (x10^3)
E h / Γ Io
0
10
20
30
40
50
10^7
10^8

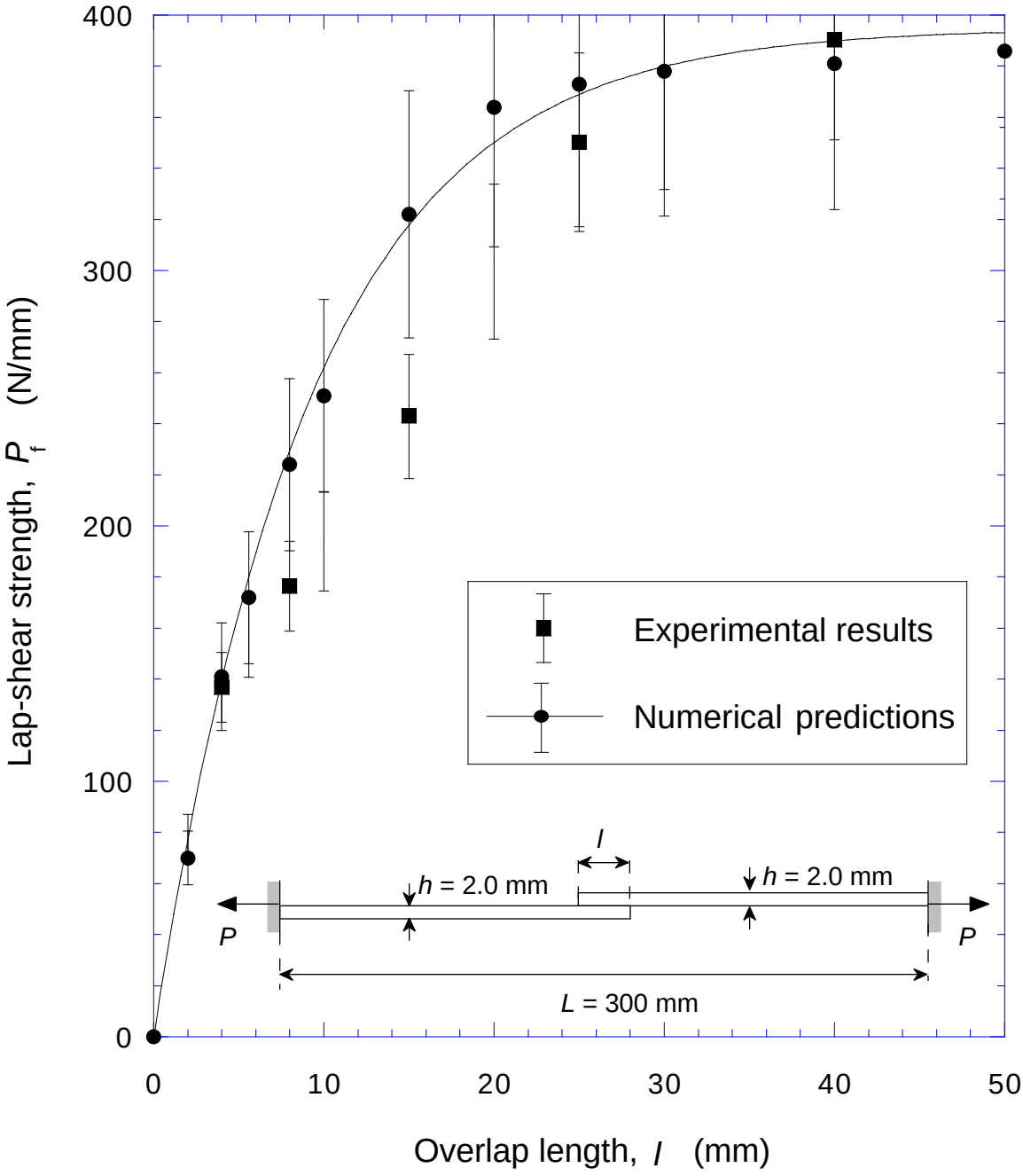
Lap-shear strength, P_f (N/mm)
Overlap length, l (mm)
0
100
200
300
400
0
10
20
30
40
50
Experimental results
Numerical predictions
l
h = 2.0 mm
h = 2.0 mm
P
P
L = 300 mm

(a)

(b)

(c)

(d)

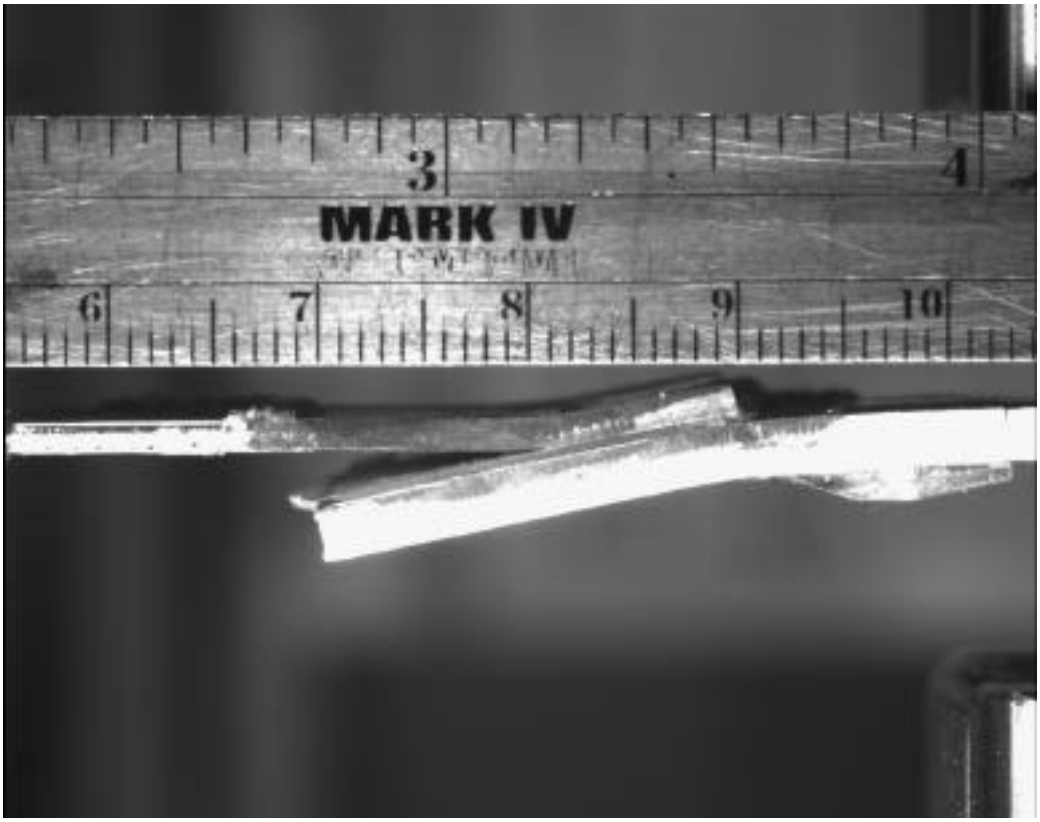

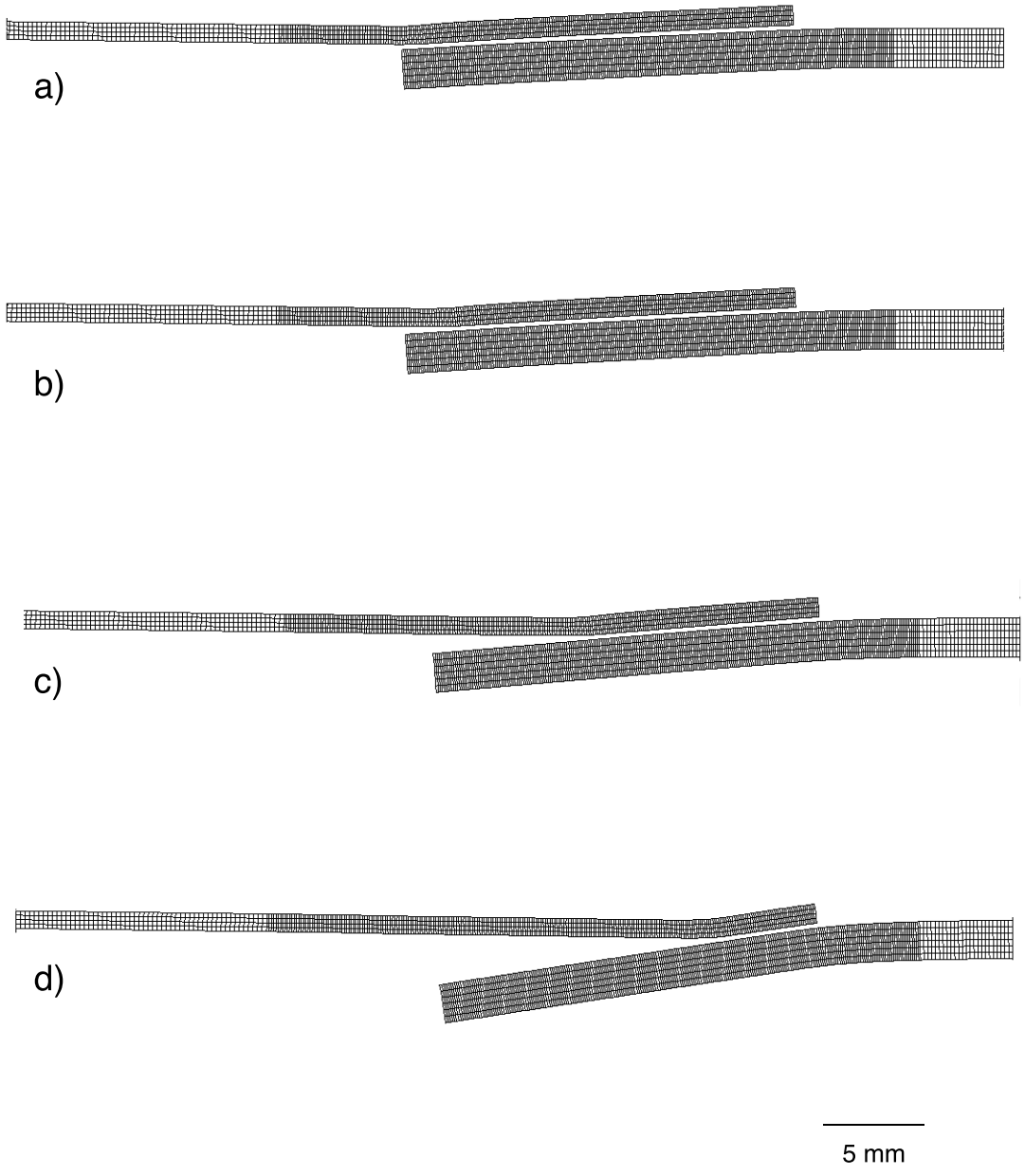
a)
b)
c)
d)
5 mm

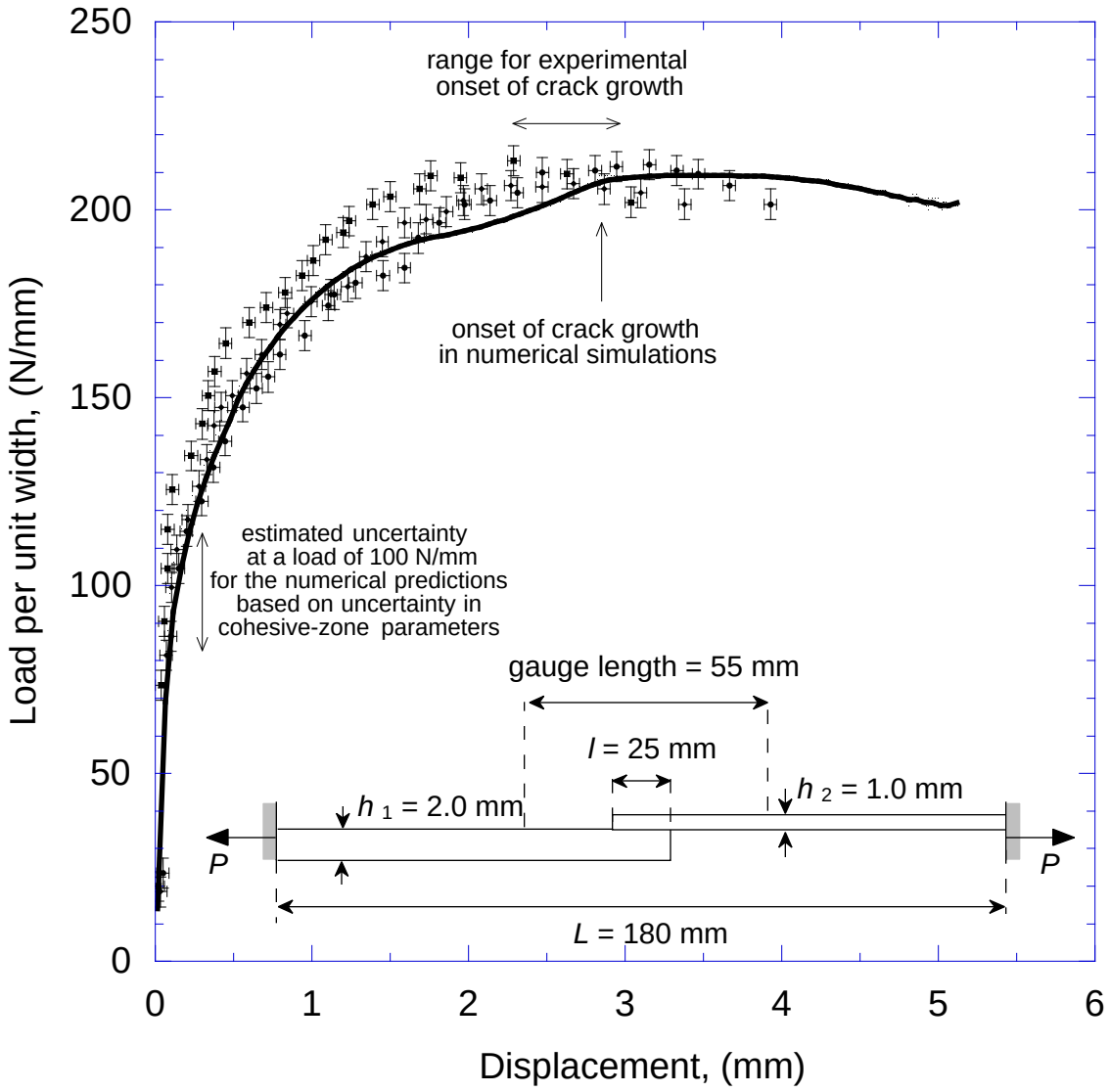
range for experimental
onset of crack growth
onset of crack growth
in numerical simulations
estimated uncertainty
at a load of 100 N/mm
for the numerical predictions
based on uncertainty in
cohesive-zone parameters
gauge length = 55 mm
l = 25 mm
h 1 = 2.0 mm
h 2 = 1.0 mm
P
P
L = 180 mm
Load per unit width, (N/mm)
Displacement, (mm)
0
50
100
150
200
250
0
1
2
3
4
5
6

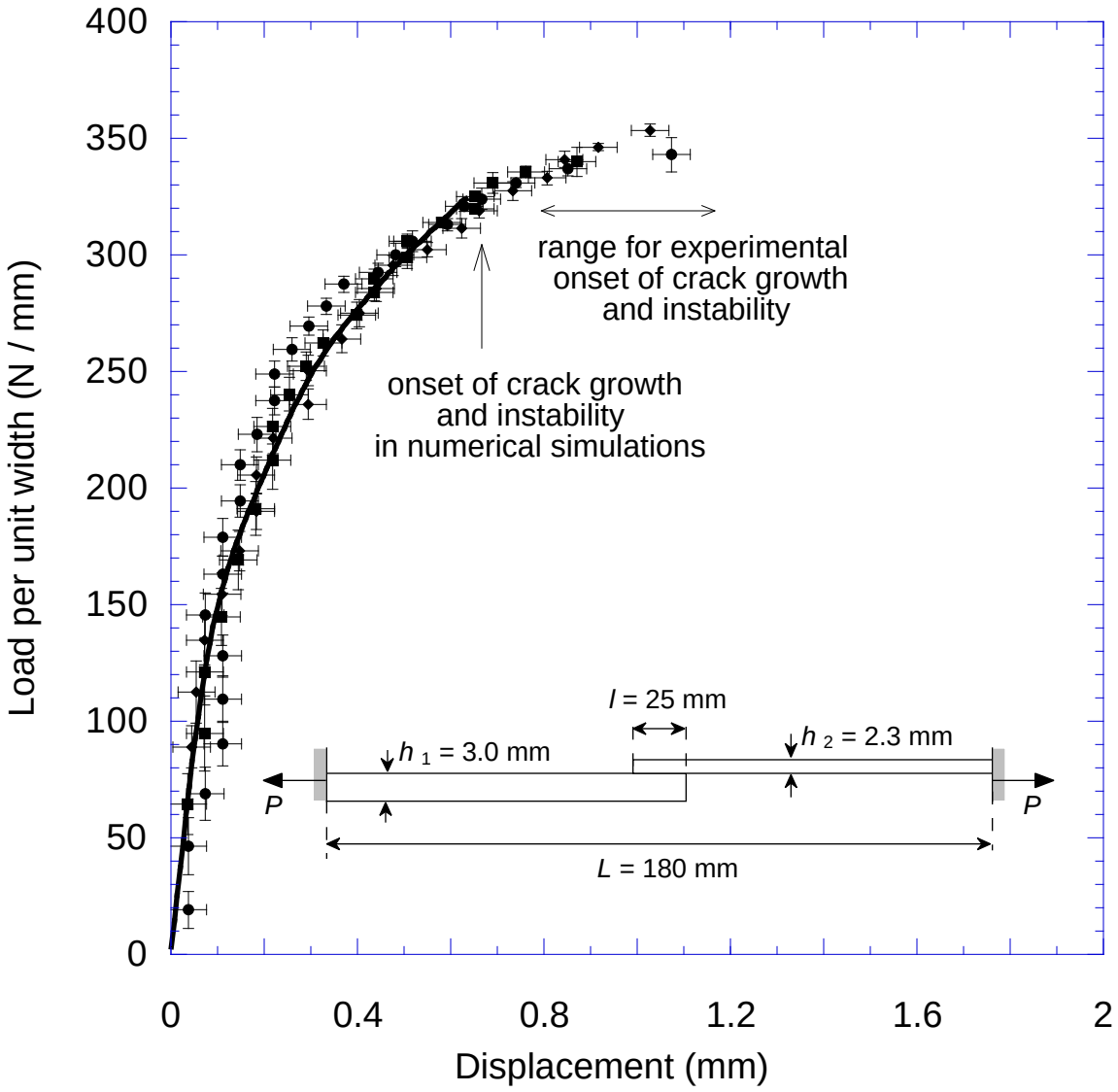
Load per unit width (N / mm)
Displacement (mm)
0
50
100
150
200
250
300
350
400
0
0.4
0.8
1.2
1.6
2
range for experimental
onset of crack growth
and instability
onset of crack growth
and instability
in numerical simulations
l = 25 mm
h 1 = 3.0 mm
h 2 = 2.3 mm
P
P
L = 180 mm